Heliyon 10 (2024) e33106

Contents lists available at ScienceDirect

Heliyon

journal homepage: www.cell.com/heliyon

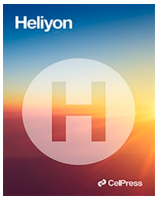

Research article

A novel nomogram model for lung adenocarcinoma subtypes based on RNA-modification regulatory genes

Xiao Chen [a], Meng-Yu Zhang [b], Xiu-Li Ji [c], Rui Li [b], Qing-Xiang Wang [b], Yi-Qing Qu [b,*]

[a] Department of Pulmonary and Critical Care Medicine, Tai'an City Central Hospital, Tai'an, China
[b] Department of Pulmonary and Critical Care Medicine, Qilu Hospital of Shandong University, Jinan, China
[c] Department of Pulmonary Disease, Jinan Traditional Chinese Medicine Hospital, Jinan, China

ARTICLE INFO

Keywords:
RNA-Modification regulatory genes (RRGs)
Risk score
A prognostic nomogram
Nonnegative matrix factorization (NMF)
Immune checkpoint

ABSTRACT

Background: In non-small cell lung cancer (NSCLC), lung adenocarcinoma (LUAD) is the most common subtype. RNA modification has become the frontier and hotspot of current tumor research.

Results: In this study, 109 genes that regulate RNA modifications were identified according to The Cancer Genome Atlas (TCGA). A differential gene expression analysis identified 46 differentially expressed RNA modification regulatory genes (DERRGs). LUAD samples were stratified into two distinct clusters based on the expression of these DERRGs. A significant correlation was observed between these clusters and patient survival rates, as well as clinical features. Furthermore, a four-DERRG signature (EIF3B, HNRNPC, IGF2BP1, and METTL3) developed using LASSO regression. According to the calculated risk scores from this signature, LUAD patients were categorized into high-risk and low-risk groups. Patients in the low-risk group exhibited a more favorable prognosis. A prognostic nomogram was crafted, integrating the four-DERRGs signature with clinical parameters. The nomogram was revealed that OS, age, clinical stage, immune cell infiltration, and immune checkpoint molecule expression were significantly linked to the OS of LUAD. GSEA analysis found that the DERRGs were primarily regulated immune pathways.

Conclusions: This study developed four DERRGs signatures and formulated a nomogram model for precise prognosis estimation in LUAD patients. The study's insights are instrumental for advancing diagnosis, prognosis, and therapeutic strategies for LUAD.

1. Introduction

Globally, lung cancer is among the most frequent and most deadly cancers [1] (Supplementary Figs. 1a and b). In 2020, an estimated 19 million new cancer cases were diagnosed, with lung cancer representing 11.4 % of these cases (Supplementary Fig. 2a). In China, lung cancer has a 17.9 % incidence rate (Supplementary Fig. 2b), marking it as the most common and deadly cancer [2]. About 85 % of lung cancer cases are NSCLC, while the remainder are small-cell lung cancer (SCLC) [3]. Currently, the incidence of LUAD, the main NSCLC subtype, has increased incidence among young women and non-smokers [4]. Despite rapid advancements in diagnostic methods and targeted and immunotherapy for LUAD, not all patients benefit from these treatments, and difficulties in early diagnosis

* Corresponding author. Department of Pulmonary and Critical Care Medicine, Qilu Hospital of Shandong University, Jinan, 250012, China.
E-mail address: quyiqing@sdu.edu.cn (Y.-Q. Qu).

https://doi.org/10.1016/j.heliyon.2024.e33106
Received 4 August 2023; Received in revised form 7 June 2024; Accepted 13 June 2024
Available online 14 June 2024

Abbreviations

NSCLC	non-small cell lung cancer
LUSC	lung squamous cell carcinoma
LUAD	lung adenocarcinoma
RRGs	modification regulatory genes
TCGA	The Cancer Genome Atlas
DERRGs	differentially expressed RNA modification regulatory genes
NMF	Non-negative matrix factorization
SCLC	small-cell lung cancer
m6A	N6-methyladenosine
m6Am	2-O-dimethyladenosine
m3C	3-methylcytidine
m1A	N1-methyladenosine
ac4C	N4-acetylcytidine
m7G	N7-methyladenosine
ψ	pseudouridine
m5C	5-methylcytosine
OS	overall survival
AUC	area under the curve
RMS	restricted mean survival
CAR-T	chimeric antigen receptor T-cell
DCA	decision curve analysis
DCs	Dendritic cells
ROC	receiver operating characteristic
PFS	progression-free survival
GSEA	Gene Set Enrichment Analysis

and drug resistance often lead to poorer prognosis [5]. Hence, identifying new targets or immunotherapies is crucial for improving the prognosis of LUAD patients.

Epigenetic changes, such as histone alterations, RNA modification and DNA methylation, have been extensively researched, and DNA methylation has been well-documented. As the field of epigenetics progresses, RNA modification has gained recognition for its significant influence on biological functions and tumor pathology. It affects mRNA stability and expression, encoding tumor suppressor genes to reduce their anti-cancer effect, increasing the stability and expression of oncogenes, and participating in tumor initiation and progression [6,7]. As a frontier in epigenetics, RNA modification has attracted considerable research interest in recent years. Writers, erasers, and readers form an intricate regulatory network for RNA modification, as do histone modifications and DNA modifications [8].

Over 170 distinct modifications of RNA have been identified to date [9]. Transcription, splicing, translation, and stability of RNA are all controlled by these modifications. They are linked to key cancer-related processes such as metastasis, epithelial-mesenchymal transition (EMT), cell proliferation, and invasion [3]. Several important modifications, such as N6-methyladenosine (m6A) [10–12], 2-O-dimethyladenosine (m6Am) [13,14], N1-methyladenosine (m1A) [15,16], 3-methylcytidine (m3C) [17], N4-acetylcytidine (ac4C) [18], 5-methylcytosine (m5C) [19], N7-methyladenosine (m7G) [20], and pseudouridine (ψ) [21], have been found in both mRNAs and noncoding RNAs(lncRNA). Each modification has distinct classes of writers, erasers, and readers. For instance, m6A writers include WTAP, METTL3, and METTL14; the eraser is FTO; and the readers are YTHDC1, YTHDC2, YTHDF1, YTHDF2, HNRNPC, and others [10–12]. However, for some RNA modifications, the responsible 'writers', 'erasers', and 'readers' have yet to be discovered.

The burgeoning field of RNA modification research has uncovered the pivotal roles of numerous RRGs in the etiology and progression of LUAD. A case in point is METTL3, which has been demonstrated to enhance tumorigenesis and suppress ferroptosis by stabilizing the m6A modification of the SLC7A11 gene in LUAD [22]. Down-regulation of the FTO/PHF1 axis has been shown to increase the expression of FOXM1, thereby promoting the progression of LUAD [23]. The upregulation of IGF2BP3 has also been noted, with its overexpression being a harbinger of a grim prognosis in LUAD [24]. Through the AKT/mTORC1 signaling pathway, METTL1 controlled cell autophagy and proliferation in A549 cells [25]. Therefore, RRGs may offer potential as valuable prognostic indicators and may be instrumental in predicting treatment outcomes for LUAD.

Numerous prognostic models leveraging RRGs have been successfully constructed using tumor research databases, revealing potential clinical relevance for forecasting patient outcomes and guiding the development of molecularly targeted therapies. Nonetheless, a prognostic model specific to LUAD is still lacking. In this study, we have pioneered the creation of a prognostic nomogram model tailored to four RRGs for LUAD. This model not only prognosticates patient outcomes but also stratifies patients into distinct categories. Furthermore, we delved into its association with the immune profiles of LUAD patients, aiming to uncover deeper insights into the interplay between RRGs and immune responses in LUAD.

2. Materials and methods

2.1. Data collection

TCGA (https://portal.gdc.cancer.gov/) provided the clinical data for LUAD patients, including progression-free survival (PFS), survival status, and survival duration. Moreover, the mRNA expression levels of 109 RRGs (m6A, m6Am, m1A, m3C, ac4C, ψ , m5C, and m7G) were acquired from the TCGA database, and these data were subsequently converted to FPKM values. The 109 RRGs included m6A regulators, m6Am regulators, m1A regulators, m3C regulators, m5C regulators, m7G regulators, and ψ regulators.

For the datasets from the Gene Expression Omnibus (GEO, https://www.ncbi.nlm.nih.gov/geo/), the criteria for patient inclusion were: (1) the presence of LUAD patient samples within the dataset; (2) the use of RNA-sequencing or gene microarray technology; (3) the inclusion of relevant clinical survival data. Conversely, datasets were excluded from the GEO analysis if they: (1) lacked LUAD tumor data; (2) lacked survival data; (3) miRNA microarray or methylation data or other data types. Ultimately, the GSE26939 dataset, retrieved from GEO, was utilized to corroborate the prognostic value of LUAD features in the external validation cohort.

2.2. Screening of RNA-modification regulatory genes (RRGs) and NMF classification of molecular subsets

Genes were classified as DERRGs if they exhibited a p-value below 0.05 and a logFC with an absolute value exceeding 0.5 ($|logFC| > 0.5$). To evaluate the interactions of 46 DERRGs with RNA modifications (m6A, m6Am, m1A, m3C, ac4C, m5C, m7G, and ψ), their network was visualized with the STRING database with medium confidence >0.4 (https://stringdb.org/).

Non-negative matrix factorization (NMF), a prevalent technique for uncovering cancer molecular subtypes [26], was employed to ascertain the biological correlation within the gene expression matrix through tissue genes and samples to cluster cancer samples. Then, we constructed a LUAD molecular subtype based on 46 DERRGs through NMF clustering analysis. For this purpose, the NMF R package was used, with clusters ranging from 2 to 10 and a minimum membership of 10 for each cluster subclass. The most suitable number of clusters was identified by the dispersion degree, co-occurrence degree, and silhouette indices. With an optimal cluster number of 2, a novel subtype was constructed. Employing the "survival R″ package and the Kaplan-Meier method, we obtained OS and PFS curves for the LUAD subtypes.

2.3. Immune classification and scoring across various NMF-defined LUAD subtypes

Each sample's immune cell score was determined by the MCPcounter package using biomarkers indicative of immune cell infiltration, including cytotoxic lymphocytes, B lineage cells, Monocyte lineage, T cells, Myeloid dendritic cells, NK cells, $CD8^+$ T cells, Neutrophils, Fibroblasts, and Endothelial cells. The different NFM subtypes in LUAD patients were compared with the ggpubr R package, and violin-plots of different NFM subtypes expressed by different immune cells were drawn.

LUAD samples were divided into five groups, namely Wound healing (immune C1), IFN- γ Dominant (immune C2), Inflammatory (immune C3), Lymphocyte Depleted (immune C4) and TGF-beta Dominant (Immune C6) based on tumor immune model subtypes. Ggaluvial R was used to examine the distribution of immune subtypes among NMF clusters.

2.4. Development and verification of a prognostic model utilizing DERRGs

LASSO regression is a method of refining a model through variable selection and regularization. The degree of regularization of the LASSO regression was adjusted by the lambda parameter, which is directly proportional to the penalty strength for linear models with an increasing number of variables, thus leading to a model with a reduced set of variables. The lasso coefficients and the optimal selection of subgroups were used to formulate prognostic models. In this study, the TCGA-LUAD dataset comprising 507 patients was randomly partitioned into a test cohort (n = 151) and a training cohort (n = 356). Employing the "glmnet" package and "survival" package in R, variables were screened by LASSO regression using the outcomes of Univariate Cox regression analysis. Prognostic gene signatures were determined using the LASSO. The risk score was computed with the formula: risk score = coef1×gene expression1 + coef2×gene expression2 + coef3×gene expression3 + … + coef (n) × gene expression(n). A median risk score was used to stratify patients into high-risk and low-risk groups. In addition, the validity of the prognostic model was evaluated in the GSE validation cohort, TCGA test and training cohort, using the Kaplan-Meier method. The risk score was determined using ROC curve, which was generated with the "survivalROC" package in R [27]. Moreover, we analyzed the clinical parameters of the model groups, and $p > 0.05$ suggested that there was no deviation in clinical characteristics when the samples were grouped during model construction. In both high-risk and low-risk groups, prognostic models were evaluated using the Kaplan-Meier method.

2.5. Prognostic nomogram construction

The risk score as well as clinical parameters were used to determine if they independently predicted OS in LUAD patients using univariate and multivariate Cox regression analyses. With these elements identified as independent prognostic factors, we developed a nomogram using the"survival"and "RMS"R package to project patient survival rates for LUAD patients at 1-, 3-, and 5-years [28]. The accuracy of the noogram was determined by the calibration curves used to compare predicted and observed OS probabilities. The accuracy of various risk indicators was further assessed with a multi-index ROC curve. The correlation between various clinical factors and the risk score was scrutinized with the "limma" R package, with results visualized through the "ggpubr" R package for a

comprehensive understanding of their interplay [29].

Gene Set Enrichment Analysis (GSEA) offers a complimentary computational tool designed to parse genomic microarray data that encompasses a spectrum of gene sets with distinct functionalities. Through enrichment analysis, the mechanism of related genes can be inferred, which provides a foundational framework for subsequent molecular biology experiments and determines the direction of verification [30]. Utilizing the calculated risk scores, the patient cohort, comprising 507 individuals, was bifurcated into two group. GSEA was performed on the two cohorts of TCGA data to offer insights into the biological implications of the risk score stratification.

2.6. Comparison of prognostic models

To substantiate the precision of our predictive model, a comparative analysis was conducted against four alternative models. As a comparison of the quintet of models, Kaplan-Meier survival curves were utilized. The "survcomp" R package facilitated the computation of the concordance index (C-index) and the restricted mean survival (RMS) for each model. The C-index, an evaluative metric with a scale from 0.5 to 1.0, gauges model predictive accuracy, with higher values denoting superior predictive capabilities [31].

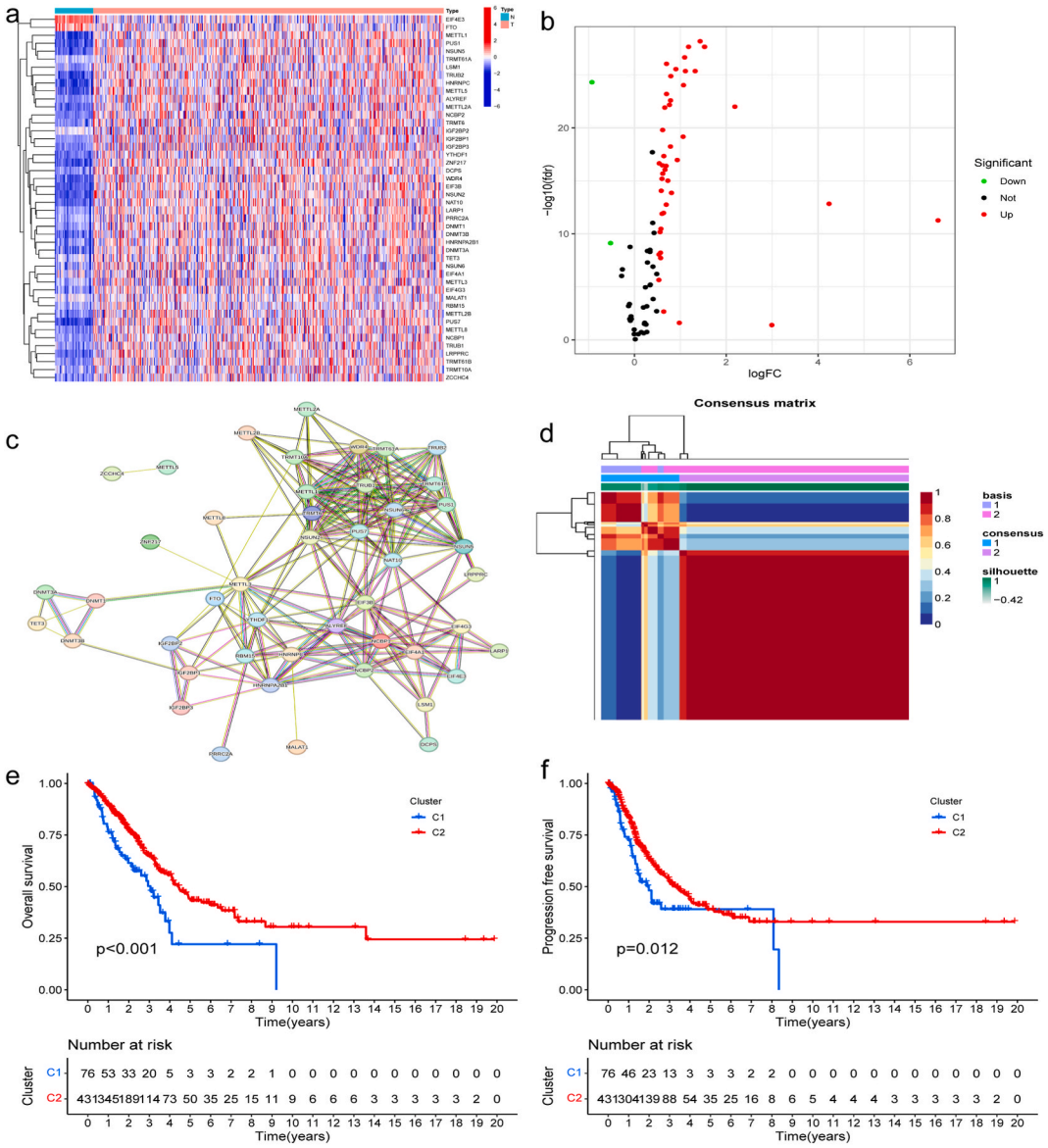

Fig. 1. LUAD subtypes based on NMF analysis. (**a, b**) Heatmap and volcano map of differentially expressed genes associated with RNA modification. (**c**) The PPI network of differentially expressed RNA modification-related genes. (**d**) NMF clustering of RNA modification-related genes. (**e**) OS analysis between two RNA modification subtypes in LUAD. (**f**) PFS analysis between two RNA modification subtypes in LUAD.

2.7. Correlations between the immune cells or immune checkpoints or TMB and the risk score

The associations between the various immune checkpoint molecules (including CD276, CD80, CD274, CD86, CTLA4, VTCN1, PDCD1, and PDCD1LG2) and risk score in LUAD patients were examined using unpaired Student's t tests. Using the "MCPcounter" in R, the frequency of tumor-infiltrating cells was determined. The immune cells of interest included B lineage, Cytotoxic lymphocytes, CD8 T cells, T cells, Monocytic lineage, NK cells, Myeloid dendritic cells, Endothelial cells, Fibroblasts, and Neutrophils. TMB scores were calculated by the Maftools R package. The correlation between immune cells and TMB was further validated by the Spearman method. Additionally, the "IMvigor" R package was used to access the IMvigor dataset, facilitating the exploration of the relationship between patient characteristics and the efficacy of immunotherapy.

2.8. Statistical analysis

We utilized R software (version 4.2.2) and Strawberry Perl for statistical analysis. For the purpose of analyzing gene expression differences, we applied the Benjamini-Hochberg procedure to manage the false discovery rate (FDR) at a significance level of $p < 0.05$. The prediction accuracy of the prognostic model was gauged by the time-dependent ROC analysis. Statistical significance is indicated by a p value less than 0.05.

3. Results

3.1. Subtypes of LUAD characterized by RRGs using NMF

In all, 109 RRGs were obtained from published articles. We used TCGA-LUAD data to determine the genes with differential expression between normal and tumor tissues, subsequently selecting 93 RRGs. A total of 46 DERRGs were identified, with 44 genes exhibiting increased expression in tumor tissue and 2 genes showing decreased expression (Fig. 1a and b; Table 1). PPI analysis was conducted on 46 DERRGs using STRING software, where the node combined score was filtered to span between 0.400 and 0.999 (Fig. 1c). Some protein-protein interactions, such as ALYREF and NCBP1, EIF4A1and EIF4G3, EIF4G3 and EIF4A1, METTL1 and WDR4, NCBP1and NCBP2, NCBP1and ALYREF, NCBP2and NCBP1, TRMT6and TRMT61A, TRMT61Aand TRMT6, and WDR4 and METTL1, had high combined_score >0.999.

In this study, cluster analysis was performed using NMF analysis. The optimal number of clusters (K) was determined through a comprehensive NMF rank survey (Fig. 2). When K = 2, two subtypes of LUAD patients were identified, and the NMF results showed a favorable match between the LUAD samples and subtypes (Fig. 3). LUAD samples (n = 507) were divided into two different subtypes (Cluster1: n = 76; Cluster2: n = 431) (Fig. 1d; Supplementary Table 1). Moreover, our analysis revealed that the LUAD patients within Cluster 2 exhibited favorable OS, contrasting with the poorer prognoses observed ($p < 0.001$, Fig. 1e). Meanwhile, patients in Cluster 1 experienced a shorter PFS compared to those in Cluster 2 ($p = 0.012$, Fig. 1f).

Table 1
46 differentially expressed RNA-modification regulatory genes (DERRGs).

gene	logFC	pValue	gene	logFC	pValue
ALYREF	0.9330	3.1E-18	METTL5	0.7624	1.3E-23
DCPS	0.6153	7.2E-17	METTL8	0.7842	1.4E-19
DNMT1	0.8063	5.4E-15	NAT10	0.7919	1.6E-26
DNMT3A	1.0602	1.6E-20	NCBP1	0.5997	2.3E-16
DNMT3B	2.1886	2.0E-23	NCBP2	0.6133	3.5E-21
EIF3B	1.0936	1.4E-28	NSUN2	1.1791	9.3E-30
EIF4A1	0.6370	1.8E-03	NSUN5	1.1095	4.9E-27
EIF4E3	−0.9266	6.8E-26	NSUN6	0.5765	1.6E-11
EIF4G3	0.6893	1.2E-17	PRRC2A	0.6008	5.7E-13
FTO	−0.5224	3.9E-10	PUS1	1.3228	4.7E-27
HNRNPA2B1	0.5391	6.6E-18	PUS7	1.4307	8.4E-31
HNRNPC	0.6983	6.8E-28	RBM15	0.5570	3.4E-11
IGF2BP1	6.6151	2.5E-12	TET3	0.5314	1.5E-06
IGF2BP2	0.9779	2.2E-02	TRMT10A	0.5673	3.5E-09
IGF2BP3	4.2384	5.9E-14	TRMT6	0.7268	3.6E-16
LARP1	0.6646	3.0E-17	TRMT61A	0.5334	5.3E-09
LRPPRC	0.7862	4.5E-24	TRMT61B	0.6090	1.1E-17
LSM1	0.6920	7.4E-14	TRUB1	0.6338	4.6E-13
MALAT1	2.9908	3.8E-02	TRUB2	0.9022	2.5E-27
METTL1	1.5297	1.1E-29	WDR4	1.0687	1.4E-25
METTL2A	0.6593	2.6E-23	YTHDF1	0.6985	1.0E-24
METTL2B	0.6393	1.2E-18	ZCCHC4	0.5829	3.3E-15
METTL3	0.5696	1.2E-08	ZNF217	1.5248	6.1E-30

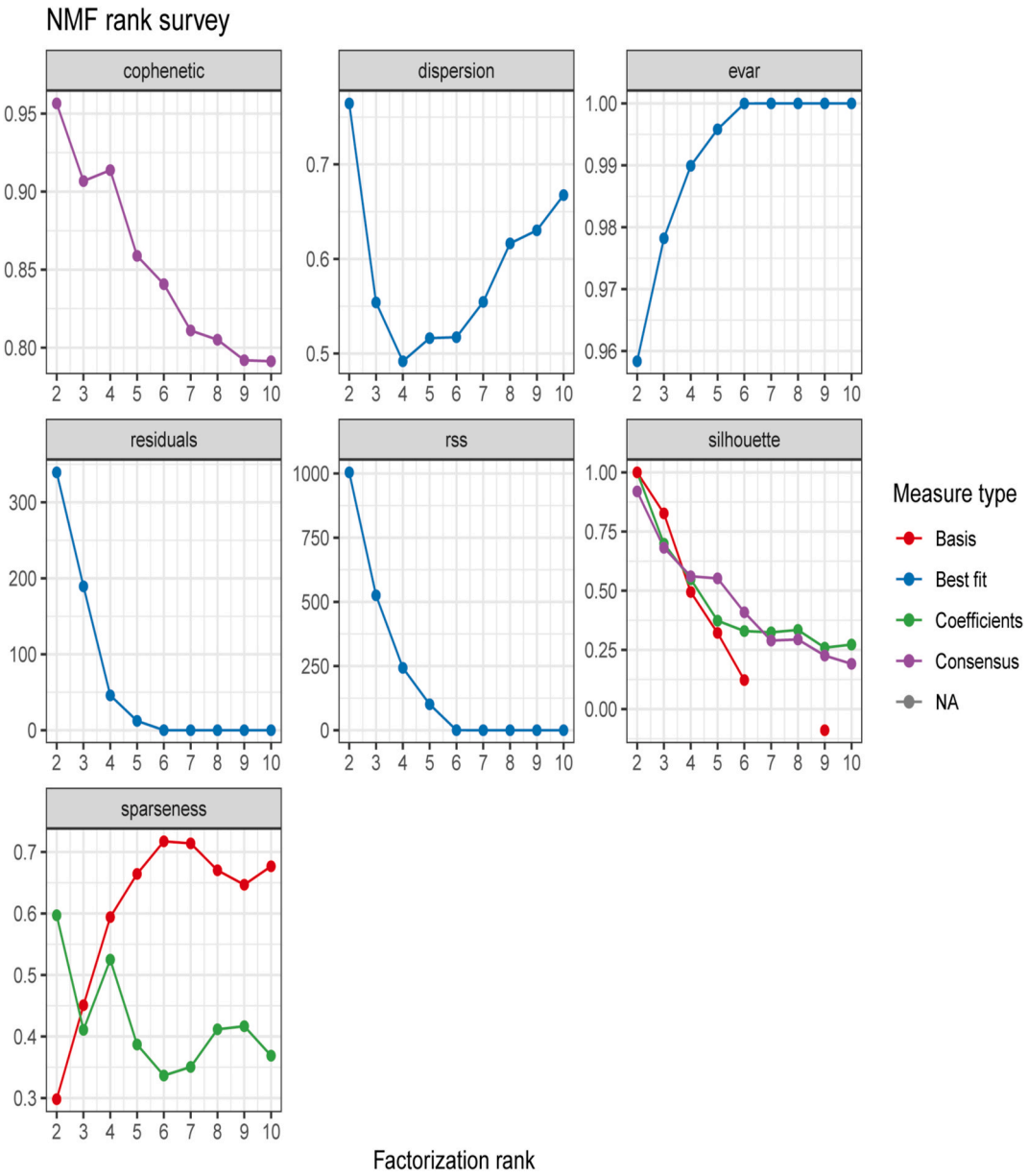

Fig. 2. Determine k value by NMF rank survey with multiparameter.

3.2. Correlations between LUAD subtypes and immune status

In this study, the associations between LUAD subtypes and immune cells, including immune cells and immune types, were analyzed. In terms of immune cell analysis, compared with Cluster 1, Cluster 2 had higher scores for endothelial cells, neutrophils, myeloid dendritic cells, and T cells (Fig. 4d, g, i, j), suggesting that there are more immune cells and a better immune response. There was no difference in expression in including Fibroblasts, CD8 T cells, B lineage, Monocytic lineage, NK cells, and Cytotoxic lymphocytes (Fig. 4a, b, c, e, f, h, $p > 0.05$). Immune type correlation analysis revealed that two subtypes were related to 5 immune cell subtypes (C1, C2, C3, C4, C6), with C4 being exclusive to Cluster2. Recent studies have delineated six immune subtypes and suggested that patients exhibiting elevated signatures of inflammatory subtypes tend to have the most favorable outcomes [32]. According to these studies, Cluster 2 has a predominant C3 inflammatory subtype (Fig. 4k).

3.3. Establishment and confirmation of a predictive model centered on four DERRGs

The predictive potential of the 46 DERRGs in LUAD patients was explored and 5 RNA modification-related genes were screened out

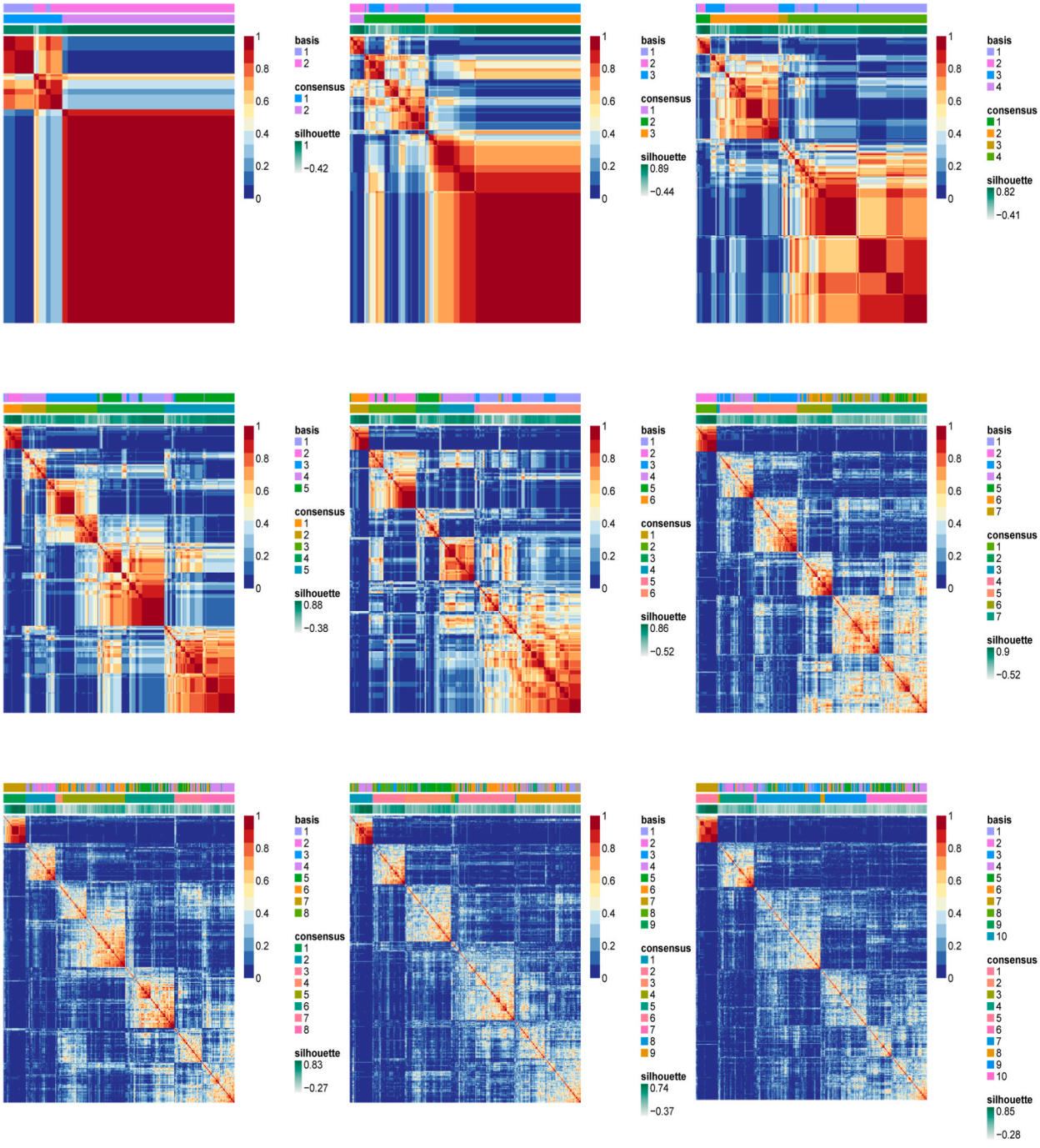

Fig. 3. NMF analysis of NSCLC cohort (K = 2–10).

($p < 0.05$) (Table 2). Next, a signature of RNA modification was constructed using four DERRGs (EIF3B, HNRNPC, IGF2BP1, and METTL3), derived from 1000 interactions identified by LASSO Cox regression analysis (Fig. 5a and b). A prognostic risk model was formulated with the risk score formula being: risk score = (0.331507057920261 × expr (EIF3B)) + (0.538210500052303 × expr (HNRNPC)) + (0.191520420170239 × expr (IGF2BP1)) + (−0.47980056864551 × expr (METTL3)).

The TCGA cohort was further divided into a validation cohort (n = 151) and a training cohort (n = 356). Clinical characteristics of the two cohorts were not significantly different (Table 3). In the TCGA cohort, the Kaplan-Meier analysis revealed a significantly shorter survival time in the high-risk group compared to the low-risk group (Fig. 5c, $p < 0.008$). In addition, the AUC values for 1, 3, and 5years were 0.669, 0.630, and 0.582, respectively, using a time-dependent ROC curve (Fig. 5f). High-risk scores were related with poorer prognoses in the training cohort (Fig. 5d, $p = 0.020$). The AUCs for the respective years, as per the time-dependent ROC curves,

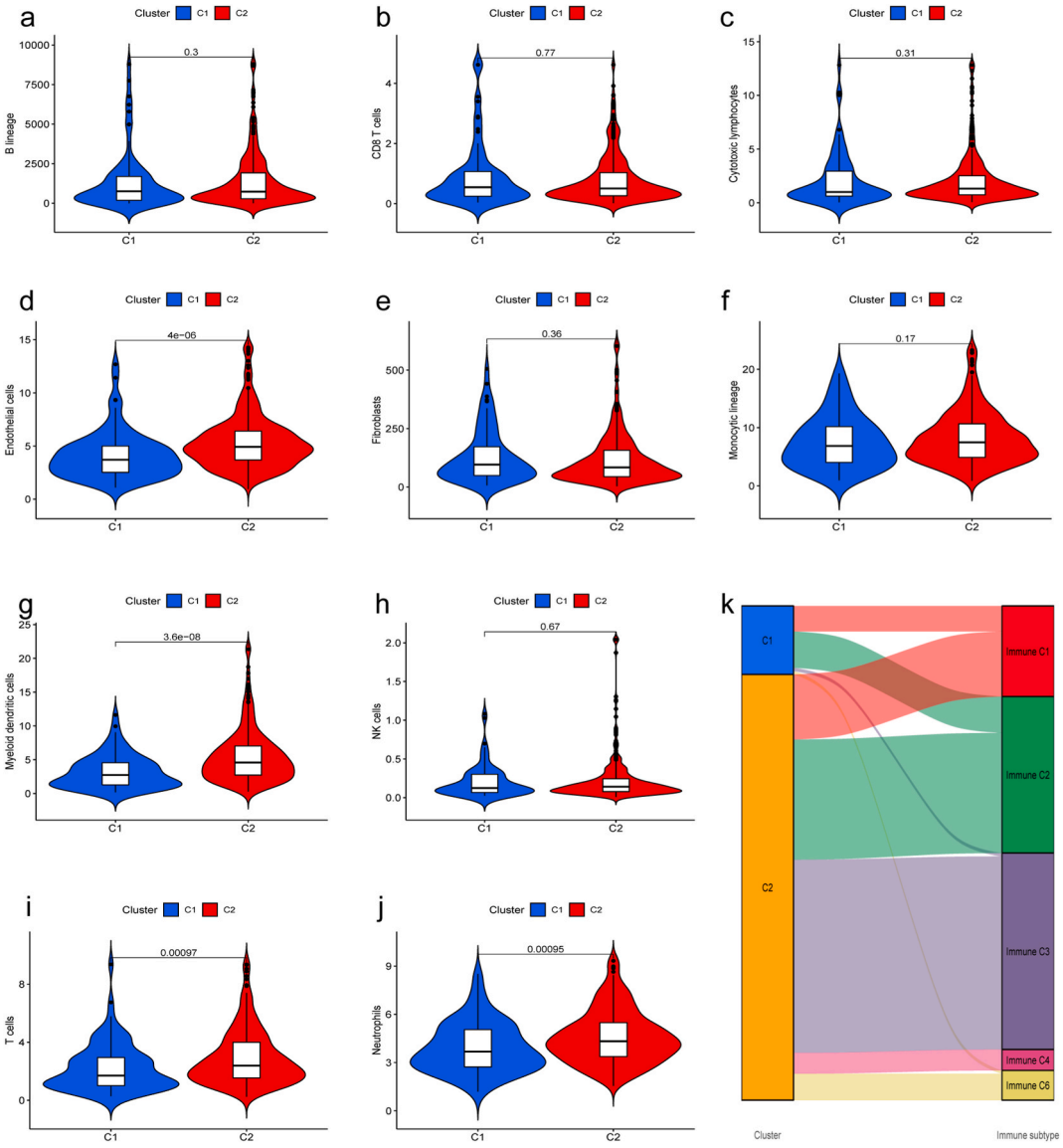

Fig. 4. Association between LUAD subtypes and immune cells or immune status. Differential expression of the two clusters in B lineage(**a**), CD8 T cells(**b**), Cytotoxic lymphocytes(**c**), Endothelial cells(**d**), Fibroblasts(**e**), Monocytic lineage(**f**), Myeloid dendritic cells(**g**), NK cells(**h**), T cells(**i**), Neutrophils(**j**). (**k**) Abundances of immune types between two clusters.

Table 2
Univariate Cox regression analysis of 46 DERRG.

id	HR	HR.95 L	HR.95H	pvalue
EIF3B	1.517094595	1.091702192	2.108245295	0.013044358
HNRNPC	1.881454839	1.174894767	3.012927125	0.008516826
IGF2BP1	1.318789269	1.134520041	1.532987584	0.000313904
IGF2BP3	1.232495302	1.04688258	1.451017238	0.0120689
METTL3	0.711467133	0.520941031	0.9716752	0.032302652

were 0.680 (1 year), 0.637 (3 years) and 0.575 (5 years) (Fig. 5g). The model's prognostic efficacy was tested in an independent TCGA test cohort, where significant differences in OS among patients of different risk groups were observed (Fig. 5e). Validation cohort AUCs at 1-year, 3-year, and 5-year were all above 0.6 (Fig. 5h). To further validate the model's accuracy across different platforms, data from GSE26938 (n = 116) was utilized. The survival rates of high-risk patients were lower than those of low-risk patients (Fig. 5i), and the AUC at 1-year, 3-year, and 5-year was 0.661, 0.581 and 0.620, respectively (Fig. 5j).

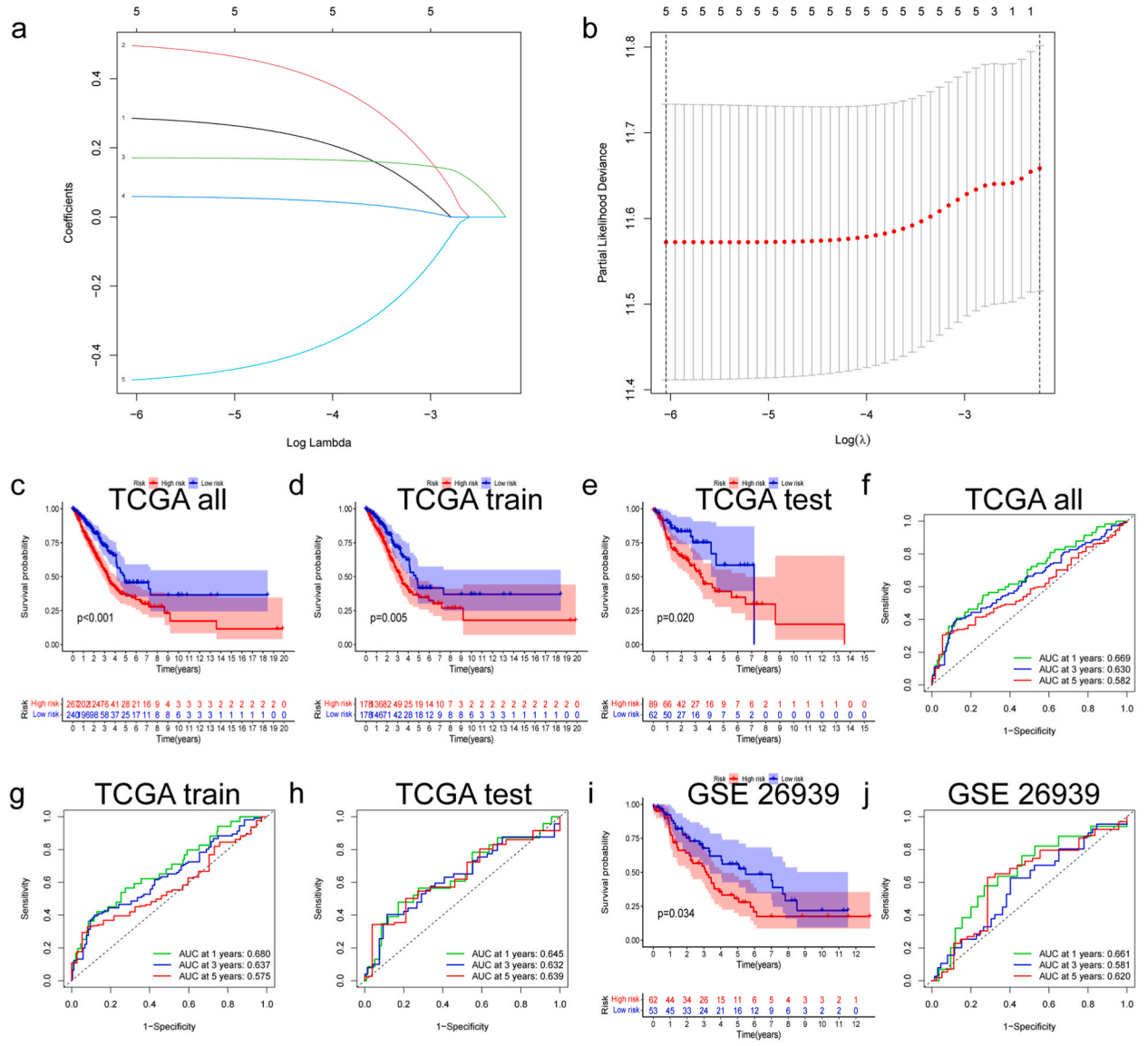

Fig. 5. Construction of prognostic model based on four DERRGs. (**a, b**). Lasso regression determined the prognostic model of lung adenocarcinoma. (**c**) OS analysis of the TCGA cohort between high risk score and low risk score group. (**d**) OS analysis of TCGA training cohort between high risk score group and low risk score group. (**e**) OS analysis of TCGA test cohort between the high-risk score group and the low-risk score group. (**f**) ROC analysis between high risk score group and low risk score group in TCGA cohort. (**g**) ROC analysis between high risk score group and low risk score group in TCGA training cohort. (**h**) ROC analysis between the high-risk score group and the low-risk score group in the TCGA test cohort. (**i**) OS analysis between the high-risk score group and the low-risk score group in the GSE26939 cohort. (**j**) ROC analysis between the high-risk score group and the low-risk score group in the GSE26939 cohort.

3.4. Correlation of the risk prediction model with clinical characteristics

Kaplan-Meier analysis showed that patients in high-risk groups had a shorter survival duration across all clinical parameters. Significant disparities were observed among different risk groups with respect to age, gender, and T stage (Fig. 6a, b, c). As illustrated in Fig. 6d, e, f, there was significantly difference in OS between the high-risk and low-risk groups only in the early stage. A low survival rate was observed in high-risk groups in N1-3, M1, and stage III-IV, although this difference did not reach statistical significance ($p > 0.05$).

As independent prognostic factors, the T stage, N stage, and the risk score were identified in univariate and multivariate Cox regression analyses (Table 4). To enhance the prediction of 1, 3, and 5 years survival rates for LUAD patients, we developed a nomogram that integrates the four gene signatures along with gender, age, T, N, M, stage, and risk score (Fig. 7a). The nomogram indicated that the risk score derived from RRGs signatures had the most substantial impact on OS in LUAD patients. Additionally,

Table 3
The clinical characteristic of TCGA test cohort and train cohort.

Covariates	Type	Total	Test	Train	Pvalue
Age	≤65	239(47.14 %)	66(43.71 %)	173(48.6 %)	0.5237
	>65	258(50.89 %)	79(52.32 %)	179(50.28 %)	
	unknow	10(1.97 %)	6(3.97 %)	4(1.12 %)	
Gender	FEMALE	272(53.65 %)	75(49.67 %)	197(55.34 %)	0.2832
	MALE	235(46.35 %)	76(50.33 %)	159(44.66 %)	
Stage	Stage I	272(53.65 %)	88(58.28 %)	184(51.69 %)	0.4548
	Stage II	120(23.67 %)	31(20.53 %)	89(25 %)	
	Stage III	81(15.98 %)	21(13.91 %)	60(16.85 %)	
	Stage IV	26(5.13 %)	9(5.96 %)	17(4.78 %)	
	unknow	8(1.58 %)	2(1.32 %)	6(1.69 %)	
T	T1	169(33.33 %)	56(37.09 %)	113(31.74 %)	0.3833
	T2	271(53.45 %)	75(49.67 %)	196(55.06 %)	
	T3	45(8.88 %)	12(7.95 %)	33(9.27 %)	
	T4	19(3.75 %)	8(5.3 %)	11(3.09 %)	
	unknow	3(0.59 %)	0(0 %)	3(0.84 %)	
M	M0	338(66.67 %)	105(69.54 %)	233(65.45 %)	0.772
	M1	25(4.93 %)	9(5.96 %)	16(4.49 %)	
	unknow	144(28.4 %)	37(24.5 %)	107(30.06 %)	
N	N0	327(64.5 %)	104(68.87 %)	223(62.64 %)	0.4093
	N1	95(18.74 %)	27(17.88 %)	68(19.1 %)	
	N2	71(14 %)	16(10.6 %)	55(15.45 %)	
	N3	2(0.39 %)	1(0.66 %)	1(0.28 %)	
	unknow	12(2.37 %)	3(1.99 %)	9(2.53 %)	

calibration curve outcomes demonstrated a strong correlation between the predicted and actual survival rates (Fig. 7b). An evaluation of the predictive power of the risk model was conducted using DCA (Fig. 7c). “None” means that all samples are negative. “All” indicates all samples were positive. Fig. 7c shows the M curve was very close to the two extreme curves, which indicated that the M curve had little application value. Within a large risk threshold range, the benefit of the nomogram was greater than that of the extreme curve, so its predictive ability was the strongest. The accuracy of multiple risk indicators was further assessed using multivariable ROC curves, with the nomogram and risk score exhibiting higher precision (Fig. 7d).

No significant correlation was found between the risk score and age (Fig. 8a, $p = 0.93$). However, a robust association was found between the risk score and gender, stage, T, and N (Fig. 8b–e). Compared with male patients, female patients were inclined to have lower risk scores ($p = 0.0038$). In addition, early-stage lung cancer patients tend to have lower risk scores than those with advanced-stage cancer, especially for stages N and T. However, a higher risk score did not show a statistically significant association with tumor metastasis (Fig. 8f, $p = 0.15$).

GSEA was performed to contrast the two cohorts, yielding 40 KEGG pathways. In the high-risk cohort, five signaling pathways, namely DNA replication, proteasome, splicesome, cell cycle, and ribosomer signaling pathway, were most significantly enriched (Fig. 8g, $p < 0.05$). Conversely, in the low-risk group, RRGs were predominantly enriched in the intestinal immune network for IgA production, taste transduction, asthma, Linoleic acid metabolism, and alpha linolenic acid metabolism signaling pathways (Fig. 8h).

3.5. Comparison of predictive models

Our model was evaluated for precision, and time-dependent ROC curves and OS were drawn comparing it to previous research models. Fig. 9a–e shows the ROC curve and OS data of the five prediction models, respectively. Our model, as depicted in Fig. 9a, achieved AUC of 0.669, 0.630, and 0.582 for the 1, 3, and 5 years, respectively. Compared with prior studies’ models, our model had the highest AUC. A comparison of high- and low-risk groups based on OS analysis by Liang et al. revealed no significant differences($p = 0.058$). As shown in Fig. 9f–g, a comparison of our model with the C-index and RMS of four published risk models revealed significant superiority.

3.6. Correlations of the four DERRGs signature risk score with immune status and TMB

Immune checkpoints are promising biomarkers in cancer immunotherapy. We explored the relationship between several important immunotherapy-related genes (VTCN1, PDCD1LG2, PDCD1, CTLA4, CD86, CD276, CD80, and CD274) and the risk score. The expression correlation analysis indicated that high-risk scores were positively associated with only CD276, and negatively correlated with CTLA4, CD86, and CD80, which also suggested that high-risk scores are associated with a negative prognosis (Fig. 10a). We investigated the relationship of risk scores with immune cell types and found that risk scores based on the four DERRGs signature were negatively correlated with immune cells, such as Monocytic lineage, Endothelial cells, T cells, Myeloid dendritic cells, and Neutrophils (Fig. 10b). The TMB was positively correlated with the riskscore, B lineage, CD8 T cell, Monocytic lineage, Cytotoxic lymphocytes, and associated negatively with Myeloid dendritic cells, Endothelial cells (Fig. 10c).

This study utilized the external dataset IMvigor 210 to analyze the immunotherapy responses among patients in two risk groups.

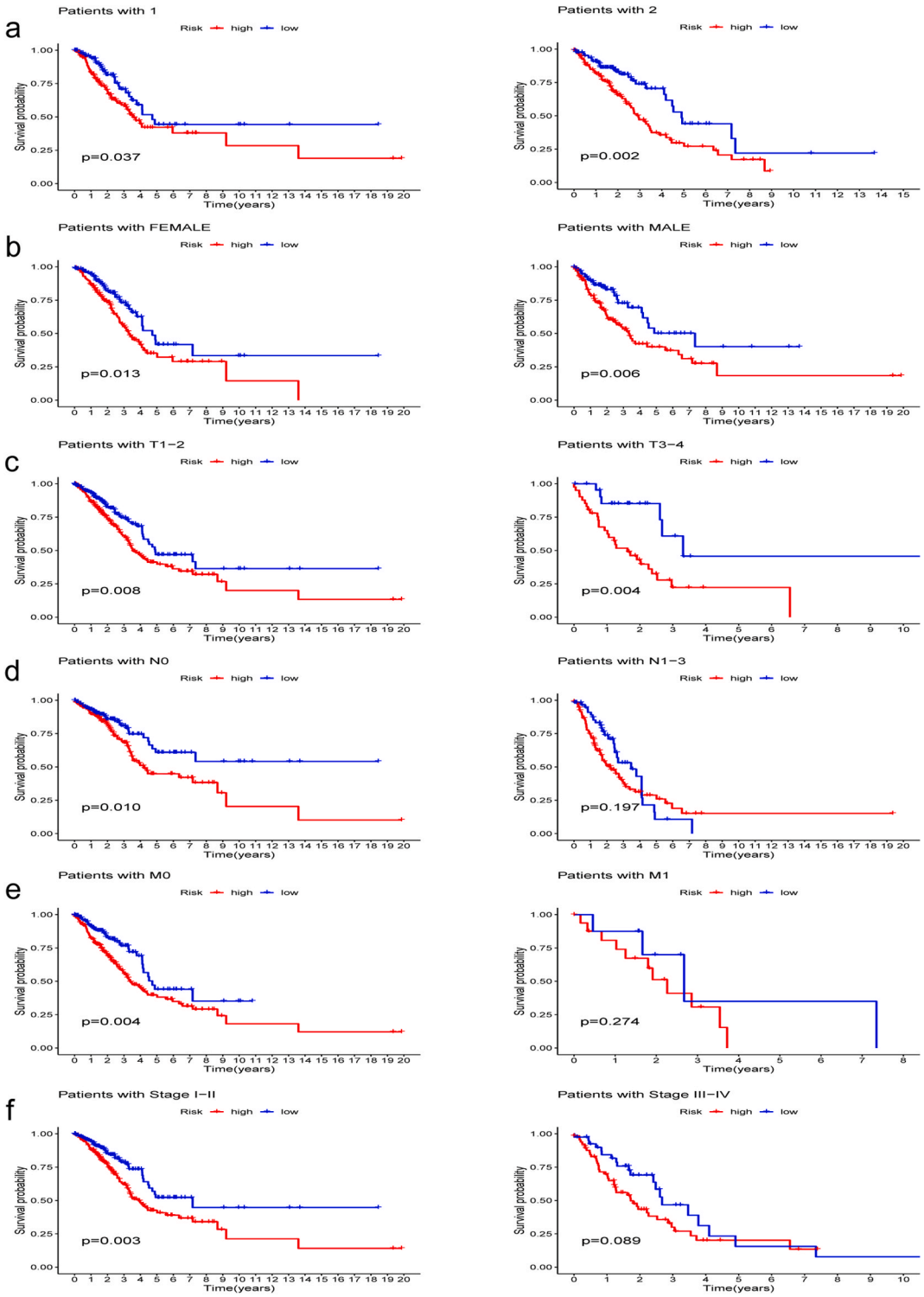

Fig. 6. Correlation of risk prediction model with clinical characteristics. (**a**) OS analysis of age between high risk score and low risk score. (**b**) OS analysis of gender between high risk score group and low risk score group. (**c**) OS analysis of T stage between the high-risk score group and the low-risk score group. (**d**) OS analysis of N stage between high risk score and low risk score. (**e**) OS analysis of M stage between high risk score group and low risk score group. (**f**) OS analysis of stage between the high-risk score group and the low-risk score group.

Table 4
Univariate and multivariate Cox regression analysis of the risk score and clinical characteristics.

	Univariate Cox regression analysis				Multivariate Cox regression analysis			
id	HR	HR.95 L	HR.95H	pvalue	HR	HR.95 L	HR.95H	pvalue
Age	1.001721	0.984325	1.019424	0.847468				
Gender	1.130499	0.810201	1.577420	0.470504				
T	1.618931	1.330278	1.970218	1.52E-06	1.286421	1.038382	1.593711	0.021190
M	1.877027	1.05793171	3.330302	0.031360	1.569172	0.876641	2.808789	0.129331
N	1.734951	1.429654	2.105444	2.41E-08	1.456971	1.176803	1.803840	0.000552
riskScore	1.917676	1.559855	2.357580	6.44E-10	1.680814	1.342457	2.104453	5.96E-06

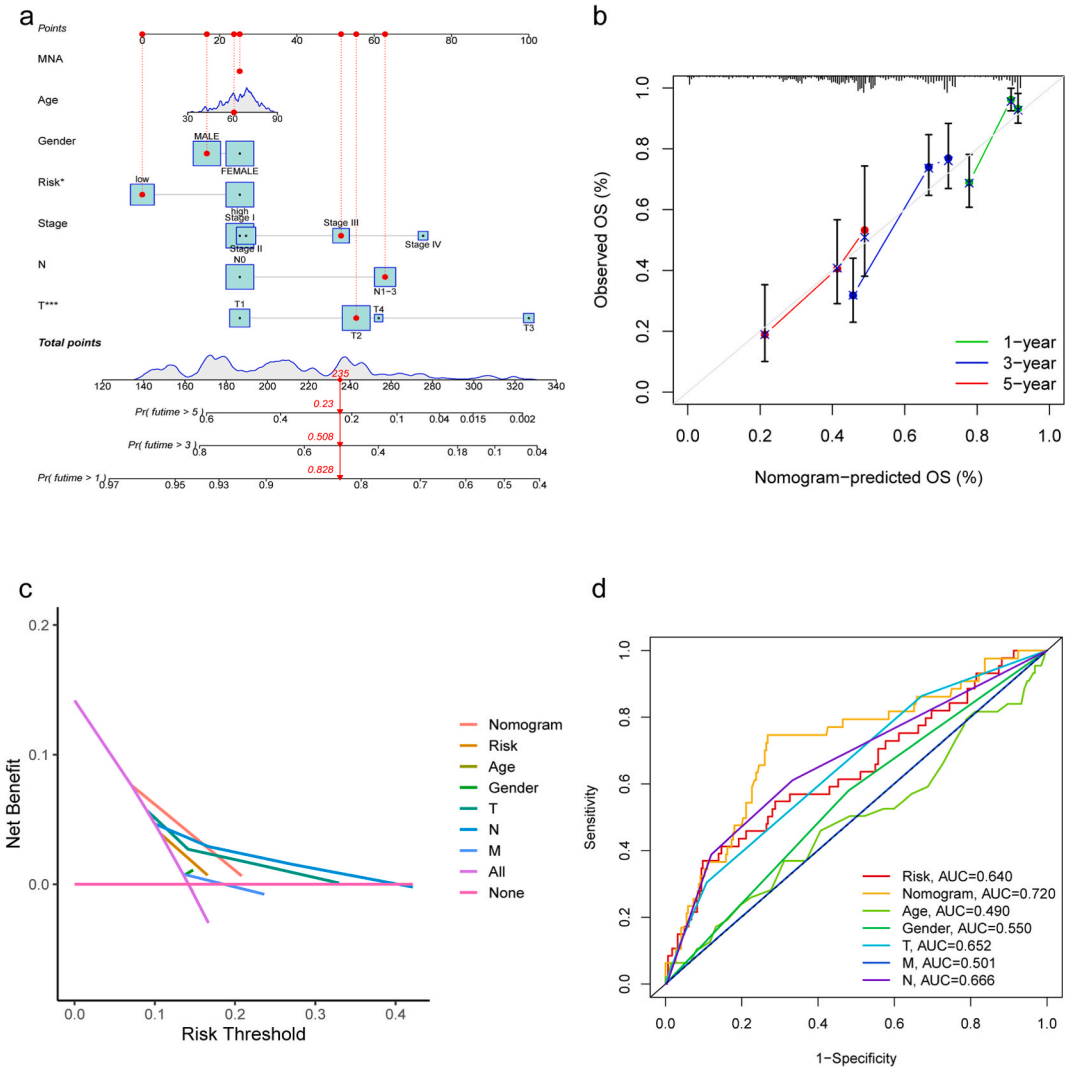

Fig. 7. A nomogram to predict overall survival probability (OS) based on DERRGs signatures and clinical factors. (**a**) Risk score evaluation nomogram for assessing prognosis in LUAD (1-year, 3-year, and 5-year survival rate). (**b**) Decision tree diagram of Nomogram. (**c**) Decision curve analysis for nomogram, risk and clinicopathological prognostic indicators. (**d**)Multi-indicator ROC curves for risk score and other metrics.

The AUCs of RRGs features at 1, 3, and 5 years were 0.701, 0.596, and 0.526, respectively (Fig. 11a). The KM curve revealed that in the low-risk group, according to the IMvigor 210 dataset, patients exhibited a longer OS compared to other patients (Fig. 11b). SD/PD patients had a lower risk score than CR/PR patients (Fig. 11c). Patients who did not receive platinum-based therapy had a lower risk score (Fig. 11d). In addition, patients with early Subtype stage had a lower risk score (Fig. 11f). However, there were no model differences in the risk scores for smoking, censOS, and Sex (Fig. 11e–g, 1h).

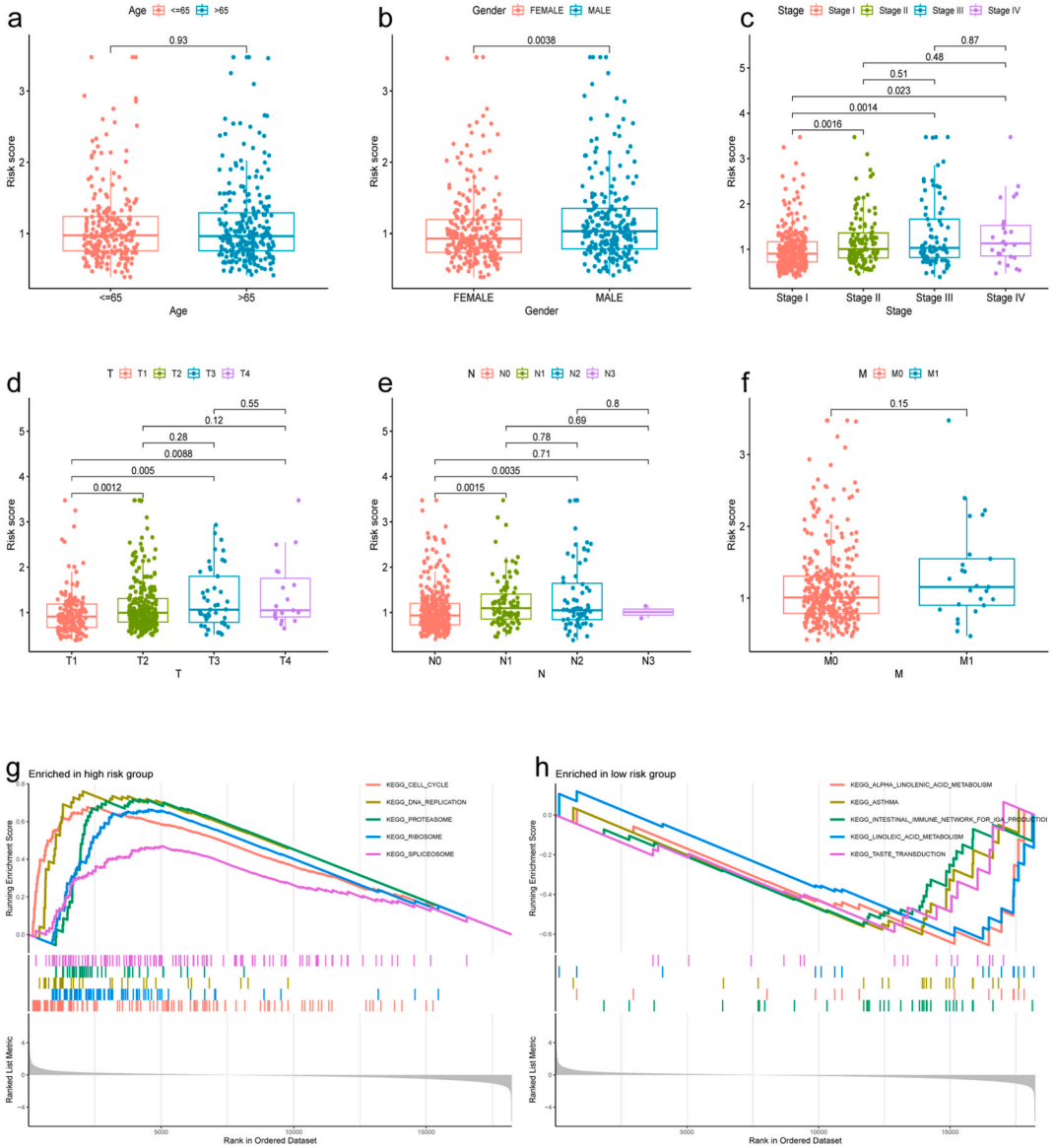

Fig. 8. Relationship between clinicopathological factors and risk score. The Relationship between risk score and age (**a**), gender (**b**), stage (**c**), T(**d**), N (**e**), M (**f**). (**g–h**) GSEA analysis in the high-risk and low-risk group.

4. Discussion

Cancer is a disease characterized by genetic and epigenetic factors within various oncogenes and tumor suppressor genes. Studies have revealed that RNA modifications are crucial in controlling cancer growth [6]. The abnormal levels of enzymes that regulate RNA modifications are linked to critical cancer characteristics such as cell differentiation, proliferation, therapeutic resistance, invasion, and survival [7]. At present, the influence and underlying processes of RNA modification in lung cancer are among the research hotspots in tumor biology. The emergence and progression of various of lung cancer are related to the different functions of RNA modification [33]. Most of the regulatory proteins associated with RNA modification in tumor tissue and adjacent tissues are highly expressed and are correlated with a negative clinical outcome [34]. These regulatory proteins have great research value, and their unique molecular traits can serve as standalone indicators for the prognosis of LUAD.

Patients with LUAD currently have inadequate predictive signals for prognosis. Bian et al. used bioinformatics to identify CXC chemokines linked to the risk of LUAD and developed a prognostic risk model based on these chemokines [35]. Cancer-Related Genes (CRGs) were used to predict OS in LUAD patients by Chen et al. [36]. Liang et al. built a prognostic model centered on genes associated with circulating tumor cells and examined the relationship between DEGs and tumor immunity [37], while Zhang et al. constructed a risk model based on genes XRCC4/5/6 to anticipate the progression of LUAD [38]. With the aim to enhance LUAD prognostic models,

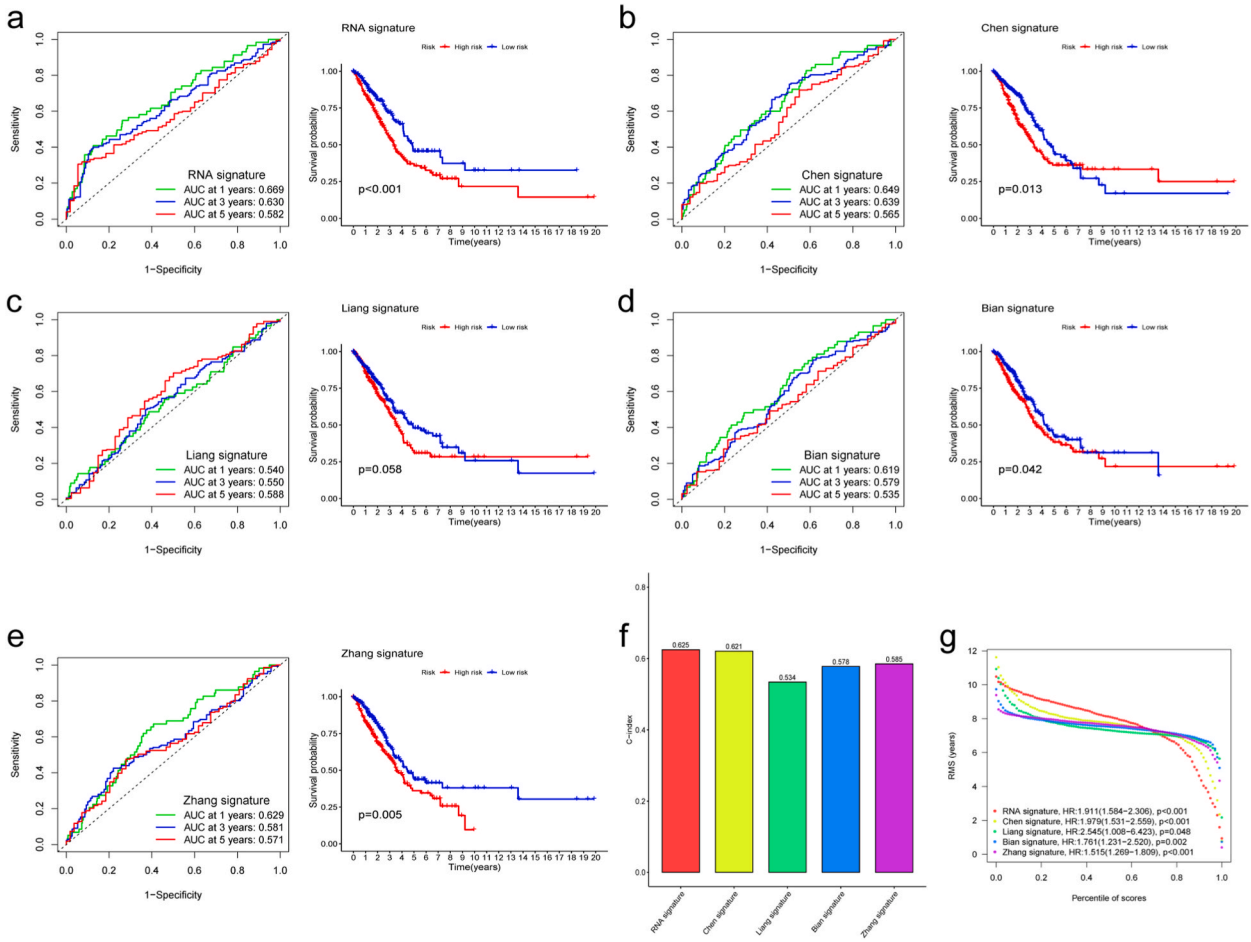

Fig. 9. Excellent predictive performance of RRGs model. (**a**) ROC and OS in the high- and low-risk groups in RNA signature. (**b**) ROC and OS in the high- and low-risk groups in Chen signature. (**c**) ROC and OS in the high- and low-risk groups in Liang signature. (**d**) ROC and OS in the high- and low-risk groups in Bian signature. (**e**) ROC and OS in the high- and low-risk groups in Zhang signature. (**f**) Comparison of C-index among risk models. (**g**) Observations of RMS among risk models.

we amalgamated data from genes associated with various RNA modifications, such as m6A, m1A, m5C, m6Am, m3C, m7G, ac4C, and ψ, to construct RNA modification-based prognostic signatures, and determine their prognostic significance and their correlation with the immune profile. In Fig. 9, we compared our model with previous research models to observe its accuracy. For 1-year, 3-year, and 5-year predictions, our model had an AUC of 0.669, 0.630, and 0.582. Our model exhibited the highest area under the curve, indicating superior predictive ability for patient survival compared to previous models. Notably, for both 1-year and 3-year predictions, AUC values surpassed 0.6, demonstrating their predictive value. However, the AUC of 0.582 for 5-year survival may be influenced by factors such as differences in data distribution or limited sample sizes in the validation and testing datasets. As standalone factors, these markers could improve the prognosis of LUAD patients, paving the way for innovative immunotherapeutic strategies aimed at LUAD.

Based on the expression of RRGs, we classified patients with LUAD into two clusters. The OS and PFS of the two clusters were different, and cluster 2 had a better prognosis. These two clusters showed the associations with immune cells (Myeloid dendritic cells, Endothelial cells, Neutrophils, T cells). Endothelial cells, which are part of the stroma, are found in the tumor microenvironment. They interact with tumor cells that have infiltrated normal epithelial cells, produce cytokines and growth factors, and thereby influence the surrounding microenvironment [39]. T cells, a crucial component of lymphocytes, are integral to cellular immunity and are a key target for tumor immunotherapy. There has been evidence that tumors containing more T cells have a better prognosis [40]. Dendritic cells (DCs), essential partners to T cells, are required to initiate adaptive immune responses. Understanding how DCs infiltrate tumors and become activated could reveal new avenues for therapeutic intervention [41]. Even though significant progress has been made in understanding neutrophil heterogeneity, biology, and function, their role in cancer remains unclear [42]. Considering the correlation of RNA modifications with the prognosis of lung cancer and tumor immunity, we deduced that genes related to the regulation of RNA modifications could be potential biomarkers for evaluating prognosis and immunotherapy response.

By LASSO regression analysis, four DERRGs (EIF3B, HNRNPC, IGF2BP1, and METTL3) that were significantly linked to an unfavorable prognosis in LUAD patients were developed a prognosis model. Both the training and validation datasets showed a correlation

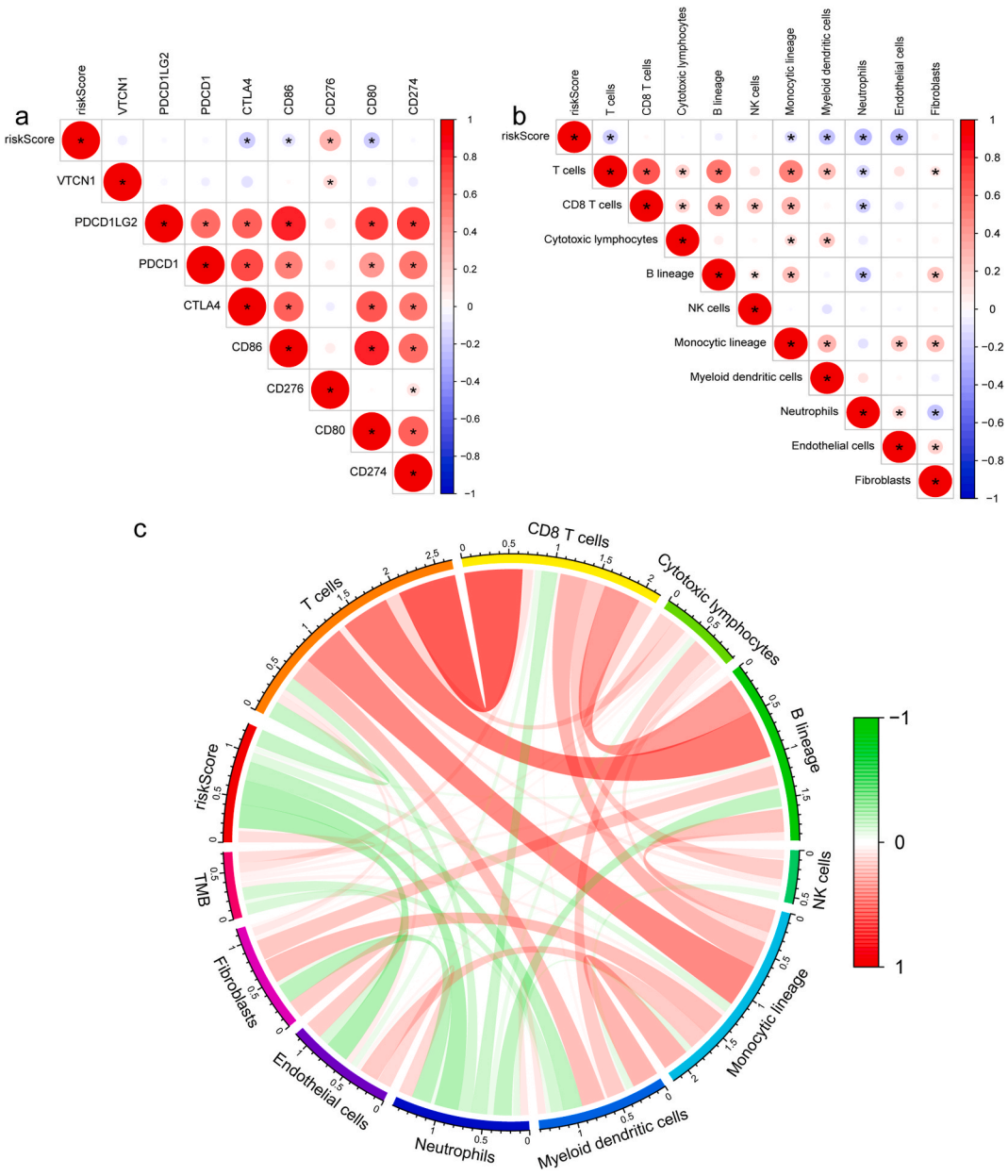

Fig. 10. Immune and TMB between high and low risk score groups. (**a**) Correlation between risk score and immune checkpoints. (**b**) Correlation between risk scores and immune cells. (**c**) Correlation between TMB and immune cells. *p < 0.05.

between OS and the subgroups, indicating that our model was effective at predicting LUAD patient survival. The robustness of our model was further substantiated by validation using independent cohorts from the GSE26939 and IMvigor 210 databases. The external validation cohort yielded results that aligned with those of the internal validation cohort, further suggesting that our model was a reliable tool for assessing the response and prognosis of LUAD to immunotherapy. In addition, we also found significant correlations among age, sex, T, N, M, stage and risk groups. A multivariate and univariate Cox regression analysis was carried out establish the prognostic model's independence. In LUAD patients, T, N, and risk score were independent prognostic factors. Developed a nomogram chart that includes gender, age, stage, T, N, and risk score to predict LUAD prognosis. Based on constructed ROC curve, the nomogram had the highest AUC, followed by T and N. Compared with other prognostic models [36–39], our prediction model had greater accuracy. This new model for prognostic scoring of LUAD patients offered a valuable tool for patient staging and clinical management.

Among the four DERRGs (EIF3B, HNRNPC, IGF2BP1, and METTL3) in prognostic models, METTL3 has been extensively studied in LUAD. METTL3 plays an oncogenic role in LUAD progression [22]. Elevated levels of HNRNPC have been detected in LUAD tissues and cells, with an increase in its expression correlating inversely with the OS and DFS of LUAD patients [43]. Similarly, the overexpression

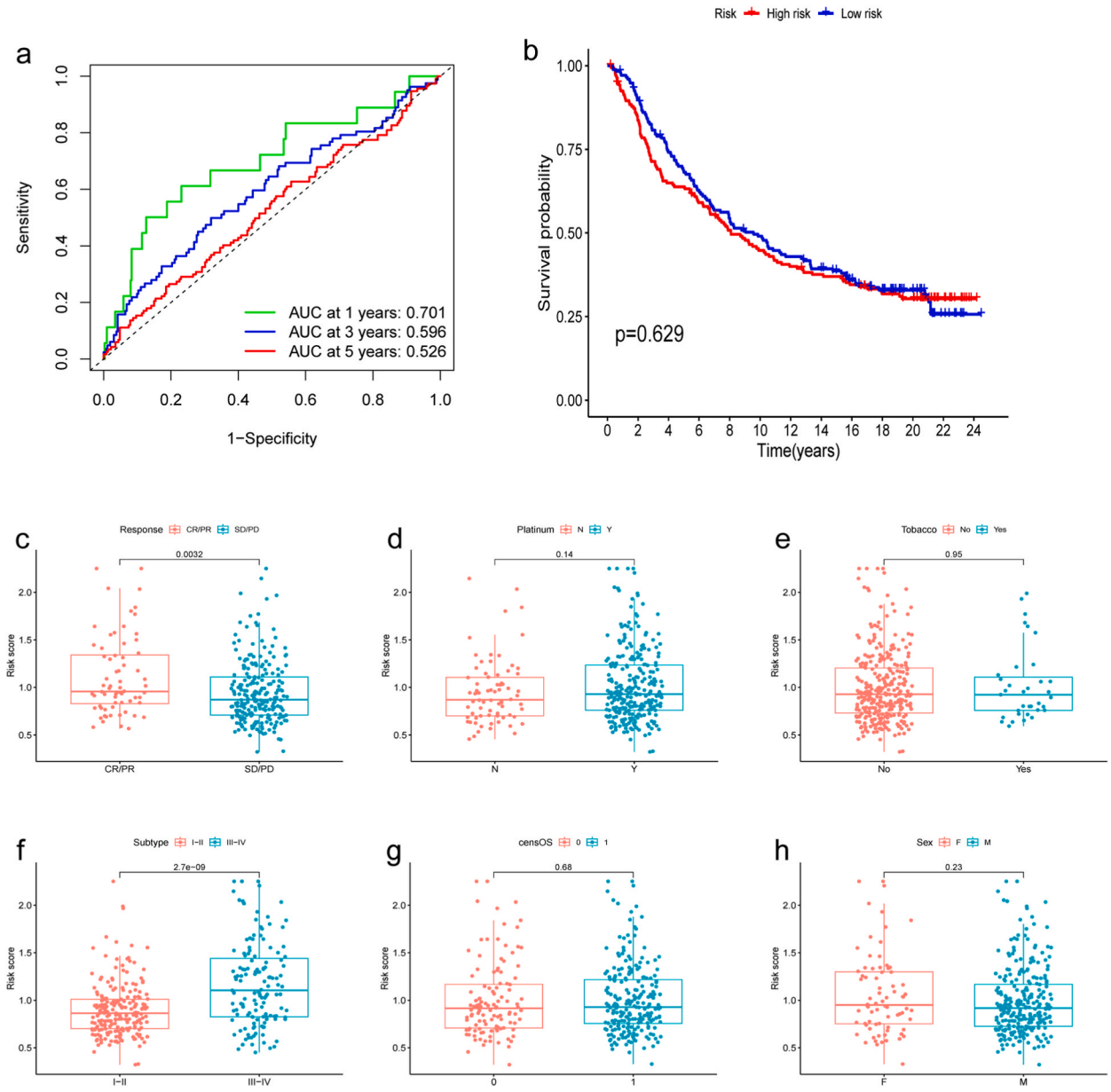

Fig. 11. Immunotherapy responses in high-risk and low-risk groups. (**a**) ROC curves between two risk groups in the IMvigor 210 database. (**b**)K-M survival curves between two risk groups in the IMvigor 210 database. (**c**) Boxplots of risk scores in SD/PD group and CR/PR group. (**d**)Boxplots of risk scores in accept or not plalinum. (**e**)Boxplots of risk scores in Tobacco. (**f**)Boxplots of risk scores in I-II and III-IV stage. (**g**)Boxplots of risk scores in censOS. (**h**)Boxplots of risk scores in sex.

of IGF2BP1 has been linked to advanced stages of the disease and a poorer prognosis in LUAD patients [44]. Despite the lack of specific clinical studies exploring this correlation, the study emphasized the importance of EIF3B in LUAD pathology and prognosis. Considerable progress has been achieved in the practical use of immune checkpoint therapies, focusing on the modulation of T cell regulatory pathways to enhance the body's immune reaction against cancer [45]. This therapeutic approach has emerged as a novel and potent strategy in the fight against cancer [45]. The current research uncovered that CD276 acted as a distinguishing marker between high- and low-risk groups in correlation studies, indicating its critical involvement in the advancement of LUAD. Inhibitors targeting the CD276 immune checkpoint may significantly enhance the efficacy of LUAD immunotherapy. As a member of the B7 family, CD276 (B7–H3) was intricately involved in the regulation of tumor metastasis, invasion, growth, and immune evasion [46]. Given its elevated expression in various tumors and its relative scarcity in many normal tissues, CD276 has become a target of tumor gene therapy and monoclonal antibody therapy [46]. Further research and clinical trials are needed to substantiate its clinical utility as an immunotherapy target [46].

The TMB is a relatively new biomarker, that predicts the effectiveness of Immune Checkpoint Blockade (ICB) and has become instrumental in identifying patients likely to benefit from immunotherapy [47]. TMB, along with other genetic determinants of immunotherapy response, has opened up new and exciting paths toward improving the precision of cancer treatment [47]. A positive correlation was found between TMB and CD8+T cells, cytotoxic lymphocytes, riskScore, monocytic lineage, B lineage, and a negative correlation with endothelial cells and myeloid dendritic cells. The above showed that TMB can be gauged by the infiltration of immune cells, which could further refine immunotherapy strategies for LUAD patients.

This research further underscored the importance of RNA modification and its regulation in cancers, specifically LUAD. This enhanced our comprehension of how RNA modification and its regulatory mechanisms influence the immune landscape surrounding LUAD, as well as the potential impact on immunotherapy strategies. Moreover, we explored the impact of DERRGs on LUAD and their relevance to drug sensitivity. However, it is crucial to acknowledge that our study solely relied on the analysis of public databases and did not involve further validation through cell or animal experiments. Additionally, the limited sample size in public databases might have impacted the accuracy of the LASSO model. Furthermore, although we used additional databases to validate our LASSO model, there was a lack of specific clinical research exploring the correlation between the expression levels of EIF3B, HNRNPC, IGF2BP1, and METTL3 and LUAD prognosis. Future studies should focus on conducting in-depth research using real clinical samples to assess the role of DERRGs in LUAD development and their influence on patient survival.

5. Conclusion

In summary, the influence of RNA modification and its regulatory processes was profound in the genesis, advancement, and prognostic assessment of LUAD. The newly developed prognostic model based on four DERGs (EIF3B, HNRNPC, IGF2BP1, and METTL3) represented an innovative scoring system for LUAD patients. This model held great significance in terms of prognosis evaluation, patient stratification, and prediction of immunotherapy outcomes in LUAD patients.

Consent for publication

Not applicable.

Date availability statement

The datasets examined in the present study were accessible through the online databases. The latest cancer statistics from were downloaded from Cancer today (https://gco.iarc.fr/today/home). The pertinent clinical data of LUAD patients were obtained from TCGA (https://portal.gdc.cancer.gov/). GSE26939 downloaded from GEO database (https://www.ncbi.nlm.nih.gov/geo/).

CRediT authorship contribution statement

Xiao Chen: Writing – original draft, Visualization, Funding acquisition, Conceptualization. **Meng-Yu Zhang:** Investigation, Data curation. **Xiu-Li Ji:** Software. **Rui Li:** Visualization, Software. **Qing-Xiang Wang:** Visualization. **Yi-Qing Qu:** Writing – review & editing, Conceptualization.

Declaration of competing interest

The authors declare that they have no known competing financial interests or personal relationships that could have appeared to influence the work reported in this paper.

Appendix A. Supplementary data

Supplementary data to this article can be found online at https://doi.org/10.1016/j.heliyon.2024.e33106.

References

[1] J. Huang, et al., Distribution, risk factors, and temporal trends for lung cancer incidence and mortality: a global analysis, Chest 161 (4) (2022) 1101–1111.
[2] R.L. Siegel, et al., Cancer statistics, 2021, Ca - Cancer J. Clin. 71 (1) (2021) 7–33.
[3] P.C. Teng, et al., RNA modifications and epigenetics in modulation of lung cancer and pulmonary diseases, Int. J. Mol. Sci. 22 (19) (2021).
[4] X. Zhu, et al., EMT-mediated acquired EGFR-TKI resistance in NSCLC: mechanisms and strategies, Front. Oncol. 9 (2019) 1044.
[5] H.K. Choi, P.J. Mazzone, Lung cancer screening, Med Clin North Am 106 (6) (2022) 1041–1053.
[6] I. Barbieri, T. Kouzarides, Role of RNA modifications in cancer, Nat. Rev. Cancer 20 (6) (2020) 303–322.
[7] P. Nombela, B. Miguel-López, S. Blanco, The role of m(6)A, m(5)C and Ψ RNA modifications in cancer: novel therapeutic opportunities, Mol. Cancer 20 (1) (2021) 18.
[8] R. Li, et al., Prognostic value of genomic instability of m(6)a-related lncRNAs in lung adenocarcinoma, Front. Cell Dev. Biol. 10 (2022) 707405.
[9] P. Boccaletto, et al., MODOMICS: a database of RNA modification pathways. 2017 update, Nucleic Acids Res. 46 (D1) (2018) D303–d307.
[10] H. Ma, et al., N(6-)Methyladenosine methyltransferase ZCCHC4 mediates ribosomal RNA methylation, Nat. Chem. Biol. 15 (1) (2019) 88–94.

[11] T. Wang, et al., The potential role of RNA N6-methyladenosine in Cancer progression, Mol. Cancer 19 (1) (2020) 88.
[12] Y. Zhang, Y. Yang, Effects of m6A RNA methylation regulators on endometrial cancer, J. Clin. Lab. Anal. 35 (9) (2021) e23942.
[13] J. Mauer, et al., Reversible methylation of m(6)A(m) in the 5' cap controls mRNA stability, Nature 541 (7637) (2017) 371–375.
[14] M. Engel, et al., The role of m(6)A/m-RNA methylation in stress response regulation, Neuron 99 (2) (2018) 389–403.e9.
[15] Q. Zheng, et al., Genetic characteristics and prognostic implications of m1A regulators in pancreatic cancer, Biosci. Rep. 41 (4) (2021).
[16] M. Safra, et al., The m1A landscape on cytosolic and mitochondrial mRNA at single-base resolution, Nature 551 (7679) (2017) 251–255.
[17] S. Wang, et al., Integrative analysis of m3C associated genes reveals METTL2A as a potential oncogene in breast Cancer, J. Transl. Med. 20 (1) (2022) 476.
[18] D. Arango, et al., Acetylation of cytidine in mRNA promotes translation efficiency, Cell 175 (7) (2018) 1872–1886.e24.
[19] K.E. Bohnsack, C. Höbartner, M.T. Bohnsack, Eukaryotic 5-methylcytosine (m^5C) RNA methyltransferases: mechanisms, cellular functions, and links to disease, Genes 10 (2) (2019).
[20] M. Chen, et al., m7G regulator-mediated molecular subtypes and tumor microenvironment in kidney renal clear cell carcinoma, Front. Pharmacol. 13 (2022) 900006.
[21] A.A. Khan, et al., WBSCR22 and TRMT112 synergistically suppress cell proliferation, invasion and tumorigenesis in pancreatic cancer via transcriptional regulation of ISG15, Int. J. Oncol. 60 (3) (2022).
[22] Y. Xu, et al., METTL3 promotes lung adenocarcinoma tumor growth and inhibits ferroptosis by stabilizing SLC7A11 m(6)A modification, Cancer Cell Int. 22 (1) (2022) 11.
[23] J. Ning, et al., Down-regulated m6A reader FTO destabilizes PHF1 that triggers enhanced stemness capacity and tumor progression in lung adenocarcinoma, Cell Death Dis. 8 (1) (2022) 354.
[24] X. Xu, et al., IGF2BP3 is an essential N(6)-methyladenosine biotarget for suppressing ferroptosis in lung adenocarcinoma cells, Mater Today Bio 17 (2022) 100503.
[25] C. Wang, et al., Methyltransferase-like 1 regulates lung adenocarcinoma A549 cell proliferation and autophagy via the AKT/mTORC1 signaling pathway, Oncol. Lett. 21 (4) (2021) 330.
[26] P. Zheng, N. Li, X. Zhan, Ovarian cancer subtypes based on the regulatory genes of RNA modifications: novel prediction model of prognosis, Front. Endocrinol. 13 (2022) 972341.
[27] P.J. Heagerty, Y. Zheng, Survival model predictive accuracy and ROC curves, Biometrics 61 (1) (2005) 92–105.
[28] E. Núñez, E.W. Steyerberg, J. Núñez, [Regression modeling strategies], Rev. Esp. Cardiol. 64 (6) (2011) 501–507.
[29] M.J. Whitehead, et al., MyelinJ: an ImageJ macro for high throughput analysis of myelinating cultures, Bioinformatics 35 (21) (2019) 4528–4530.
[30] A. Subramanian, et al., Gene set enrichment analysis: a knowledge-based approach for interpreting genome-wide expression profiles, Proc. Natl. Acad. Sci. U.S. A. 102 (43) (2005) 15545–15550.
[31] A. Dolcetta-Capuzzo, et al., Gastroenteric neuroendocrine neoplasms classification: comparison of prognostic models, Cancer 119 (1) (2013) 36–44.
[32] V. Thorsson, et al., The immune landscape of cancer, Immunity 48 (4) (2018) 812–830.e14.
[33] X. Li, et al., Expression status and prognostic value of m(6)A RNA methylation regulators in lung adenocarcinoma, Life (Basel) 11 (7) (2021).
[34] X.F. Ni, et al., The hepatic microenvironment promotes lung adenocarcinoma cell proliferation, metastasis, and epithelial-mesenchymal transition via METTL3-mediated N6-methyladenosine modification of YAP1, Aging (Albany NY) 13 (3) (2021) 4357–4369.
[35] D. Bian, Y. Chen, Bioinformatics analysis of prognostic significance and immune characteristics of CXC chemokine family in patients with lung adenocarcinoma, Comput. Math. Methods Med. 2022 (2022) 3918926.
[36] Y. Chen, et al., Identification and validation of a novel cuproptosis-related signature as a prognostic model for lung adenocarcinoma, Front. Endocrinol. 13 (2022) 963220.
[37] L. Liang, et al., Novel circulating tumour cell-related risk model indicates prognosis and immune infiltration in lung adenocarcinoma, J Immunol Res 2022 (2022) 6521290.
[38] Q.X. Zhang, et al., The roles of risk model based on the 3-XRCC genes in lung adenocarcinoma progression, Transl. Cancer Res. 10 (10) (2021) 4413–4431.
[39] H. Choi, A. Moon, Crosstalk between cancer cells and endothelial cells: implications for tumor progression and intervention, Arch Pharm. Res. (Seoul) 41 (7) (2018) 711–724.
[40] G. Schepisi, et al., CAR-T cell therapy: a potential new strategy against prostate cancer, J Immunother Cancer 7 (1) (2019) 258.
[41] C.S. Garris, J.J. Luke, Dendritic cells, the T-cell-inflamed tumor microenvironment, and immunotherapy treatment response, Clin. Cancer Res. 26 (15) (2020) 3901–3907.
[42] C.C. Hedrick, I. Malanchi, Neutrophils in cancer: heterogeneous and multifaceted, Nat. Rev. Immunol. 22 (3) (2022) 173–187.
[43] L. Zhang, H. Peng, L. Jiang, Oncogenic role of heterogeneous nuclear ribonucleoprotein C in multiple cancer types, with a particular focus on lung adenocarcinoma, using a pan-cancer analysis and cell line experiments, J. Environ. Pathol. Toxicol. Oncol. 41 (3) (2022) 77–93.
[44] H. Wu, et al., m(6)A-binding protein IGF2BP1 promotes the malignant phenotypes of lung adenocarcinoma, Front. Oncol. 12 (2022) 989817.
[45] P. Sharma, J.P. Allison, The future of immune checkpoint therapy, Science 348 (6230) (2015) 56–61.
[46] S. Liu, et al., The role of CD276 in cancers, Front. Oncol. 11 (2021) 654684.
[47] T.A. Chan, et al., Development of tumor mutation burden as an immunotherapy biomarker: utility for the oncology clinic, Ann. Oncol. 30 (1) (2019) 44–56.